Article

Pore-Filling-Dependent Selectivity Effects in the Vapor-Phase Separation of Xylene Isomers on the Metal#Organic Framework MIL-47

Vincent Finsy, Harry Verelst, Luc Alaerts, Dirk De Vos,
Pierre A. Jacobs, Gino V. Baron, and Joeri F. M. Denayer

J. Am. Chem. Soc., **2008**, 130 (22), 7110-7118 • DOI: 10.1021/ja800686c • Publication Date (Web): 10 May 2008

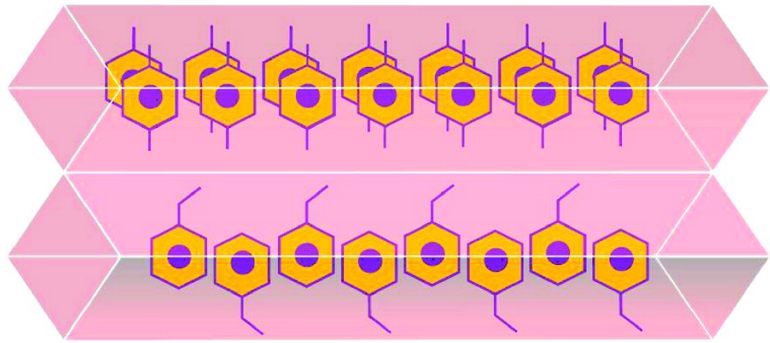

J|A|C|S
ARTICLES

Published on Web 05/10/2008

Pore-Filling-Dependent Selectivity Effects in the Vapor-Phase Separation of Xylene Isomers on the Metal−Organic Framework MIL-47

Vincent Finsy,[†] Harry Verelst,[†] Luc Alaerts,[‡] Dirk De Vos,[‡] Pierre A. Jacobs,[‡] Gino V. Baron,[†] and Joeri F. M. Denayer*,[†]

Department of Chemical Engineering, Vrije Universiteit Brussel, Brussels, Belgium, and Centrum voor Oppervlaktechemie en Katalyse, Katholieke Universiteit Leuven, Leuven, Belgium

Received January 28, 2008; E-mail: Joeri.denayer@vub.ac.be

Abstract: Vapor-phase adsorption and separation of the C8 alkylaromatic components *p*-xylene, *m*-xylene, *o*-xylene, and ethylbenzene on the metal−organic framework MIL-47 have been studied. Low coverage Henry adsorption constants and adsorption enthalpies were determined using the pulse chromatographic technique at temperatures between 230 and 290 °C. The four C8 alkylaromatic components have comparable Henry constants and adsorption enthalpies. Adsorption isotherms of the pure components were determined using the gravimetric technique at 70, 110, and 150 °C. The adsorption capacity and steepness of the isotherms differs among the components and are strongly temperature dependent. Breakthrough experiments with several binary mixtures were performed at 70−150 °C and varying total hydrocarbon pressure from 0.0004 to 0.05 bar. Separation of the different isomers could be achieved. In general, it was found that the adsorption selectivity increases with increasing partial pressure or degree of pore filling. The separation at a high degree of pore filling in the vapor phase is a result of differences in packing modes of the C8 alkylaromatic components in the pores of MIL-47.

Introduction

Xylenes are formed by toluene disproportionation, pyrolysis of gasoline, and catalytic reforming of naphtha.[1] The xylene product stream consists of four isomers: *o*-xylene (oX), *m*-xylene (mX), *p*-xylene (pX), and ethylbenzene (EB). All isomers are further processed to form a variety of products. pX, the isomer with the broadest commercial use, is used as the raw material in the manufacture of polyethylene terephtalate (PET), which in turn is used to produce polyester fibers, resins, films, and blown beverage bottles. oX is used to produce phthalic anhydride, employed as plasticizer. mX is used to produce isophthalic acid, which is gaining broader acceptance in PET resin blends, or can be isomerized (into the other isomers), and EB finally is used to obtain styrene.

Because of the economic importance and the different downstream processing of the isomers, high purity, high recovery, and high capacity are of principal interest in the xylene separation process, with typical values of respectively 99.9%, 96%, and over 21.4 million metric ton per year of pX in 2001.[2]

Because of the close matching of boiling points, separation of xylene isomers cannot be obtained by distillation, except for oX. Currently, two methods are used to achieve molecular separation: adsorption and crystallization. Recently a hybrid crystallization/adsorption process has been developed.[1] About 40% of the worldwide pX production is obtained through crystallization and 60% through adsorption.

For the separation through adsorption, the simulated moving bed technology is used.[3–7] In this way continuous streams of pure pX, mX, oX, or EB can be obtained. Industrially, xylenes are separated at around 180 °C and 9 bar.[1]

In state of the art technology, faujasite zeolites, exchanged with Na^+, K^+, and Ba^{2+}, are the only adsorbents used in the bulk-phase separation of the C8 alkylaromatic components.[8] Regarding the mechanism of xylene isomer separation on these microporous faujasites, it was shown that selectivity is determined by (i) the nature of the exchangeable cation, (ii) the composition of the mixture, (iii) the degree of pore filling, and (iv) the presence of small polar molecules like water.[8]

According to Kulprathipanja et al. and Iwayama et al., the selective adsorption of xylene isomers on faujasite zeolites is affected by the ionic potential of the exchanged cation. The isomer with the highest base strength, mX, is selectively adsorbed on the more strongly acid zeolite (NaY). Less strongly acid zeolites (KY, BaY, BaX, and KBaY) selectively adsorb the isomer having the lowest base strength, pX.[9–12]

[†] Vrije Universiteit Brussel.
[‡] Katholieke Universiteit Leuven.

(1) Minceva, M.; Rodrigues, A. E. *AIChE J.* **2007**, *53* (1), 138.
(2) Mohameed, H. A.; Jdayil, B. A.; Takrouri, K. *Chem. Eng. Process.* **2007**, *46* (1), 25.
(3) Ash, G.; Barth, K.; Hotier, G.; Mank, L.; Renard, P. *Rev. Inst. Fr. Petrol.* **1994**, *49* (5), 541.
(4) Broughton, D. B.; Chicago; Gerhold, C. G. U.S. Patent 2,985,589, assigned to UOP, 1961.
(5) Broughton, D. B.; Neuzil, R. W.; Pharis, J. M.; Brearley, C. S. *Chem. Eng. Prog.* **1970**, *66*, 70.
(6) Jeanneret, J. J. In *Handbook of Petroleum Refining Processes*, 2nd ed.; Meyers, R. A., Ed.; McGraw-Hill: New York, 1997.
(7) Otani, S.; Akita, S.; Iwamura, T.; Kanaoka, M.; Matsumura, K.; Noguchi, Y.; Sando, K.; Mori, T.; Takeuchi, I.; Tsuchiya, T.; Yamamoto, T. U.S. Patent 3,761,533, assigned to Toray Industries, Inc. , 1973.
(8) Méthivier, A. In *Zeolites for cleaner technologies*; Guisnet, M.; Gilson, J.-P., Eds.; Imperial College Press: London, 2002.

10.1021/ja800686c CCC: $40.75

For the adsorption of pX and mX on BaY and NaY, Cottier et al. observed two selective adsorption processes according to the degree of pore filling. For a filling degree lower than two molecules per supercage, the selectivity depends on the composition of the mixture: the Y zeolite is selective for the more abundant isomer in the initial adsorptive mixture, whatever the exchangeable cation. For filling higher than two molecules per supercage, the selectivity depends on the exchangeable cation: BaY selectively adsorbs pX whereas NaY selectively adsorbs mX.[13] This is in agreement with the powder neutron diffraction data of Melot et al. who observed a significant molecular rearrangement of adsorbed mX molecules when coverage is increased above two molecules per supercage in BaX zeolite. This molecular rearrangement is due to intermolecular interactions and has the goal to minimize the intermolecular repulsion.[14,15] Altogether, the confinement of the xylene isomers in a nanoscaled pore system seems necessary to achieve differences in adsorption between the different isomers which are large enough for a bulk-phase separation process to become economically viable.

A new class of micro- and mesoporous solids is formed by metal−organic frameworks (MOFs). MOFs are metal−ligand components that extend infinitely in one, two, or three dimensions and in which the ligand has to be a bridging organic group. Initially MOFs gained a huge amount of interest because of their expected large hydrogen and methane adsorption capacities.[16,17,5] Most reports on adsorption in MOFs are limited to single-component measurements of small gases such as acetylene, CO_2, N_2O, and N_2 and a number of small molecules (CCl_4, $CHCl_3$, C_6H_{12}, C_6H_6, methanol, and ethanol).[18–21] Only a few studies cover selective adsorption and use of MOFs in adsorptive separations. The potential use of MOFs for separation of alkane mixtures,[22–27] for the adsorptive removal of CO_2 and N_2O from air,[28] for the purification of CO_2−methane mixtures,[28–31] for enantioselective adsorption,[32] for the selective adsorption of organosulfur components;[33] for natural-gas cleanup, and as an efficient material for drug delivery[34] has been reported.

Only recently, the metal−organic framework MIL-47 was found to be a very effective adsorbent for the liquid-phase separation of *p*-xylene from the other xylene isomers.[35] MIL-47 is a porous terephthalate built from infinite chains of $V^{4+}O_6$ octahedra, held together by the dicarboxylate groups of the terephthalate linkers.[36] In this way a three-dimensional microporous framework with one-dimensional diamond-shaped channels with free internal diameter of about 0.85 nm is formed (see Figure 1). Every unit cell contains two channel segments.

In liquid-phase conditions, the selectivity in xylene isomer adsorption arises from differences in molecular arrangements of the adsorbed molecules in the pores of MIL-47. This was shown by Rietveld refinements of the X-ray powder diffraction patterns of MIL-47 samples saturated with each of the isomers at room temperature and in the liquid phase.[35] In such conditions, molecular packing effects become critical, given the very limited available space and freedom in the micropore.[37–42]

In the present work, adsorption and separation of xylene isomers on MIL-47 is studied under vapor conditions where the pores are less densely packed with xylene molecules. The effect of the pore-filling degree on separation efficiency is analyzed by performing breakthrough adsorption experiments.

Experimental Section

Material Synthesis and Characterization. MIL-47 was synthesized according to the method of Barthelet et al.[36] After synthesis, the excess terephthalic acid in the pores was removed by high temperature treatment at 300 °C in air. Orthorhombic crystals with diameters ranging from 0.25 to 2.0 μm were observed by scanning electron microscopy. XRD analysis of the samples revealed that the material is phase-pure MIL-47, without appreciable MIL-47as (as synthesized) or V_2O_5. The micropore volume as determined from nitrogen adsorption isotherms at the temperature of liquid nitrogen using the Dubinin−Raduskevitch method was 0.36 mL/g.

(9) Kulprathipanja, S. U.S. Patent 4,423,279, assigned to UOP, 1983.
(10) Kulprathipanja, S. U.S. Patent 5,382,747, assigned to UOP, 1995.
(11) Kulprathipanja, S.; Johnson, J. A. *Handb. Porous Solids* **2002**, 2568.
(12) Iwayama, K.; Suzuki, M. *Stud. Surf. Sci. Catal.* **1994**, *83*, 243.
(13) Cottier, V.; Bellat, J. P.; SimonotGrange, M. H.; Méthivier, A. *J. Phys. Chem. B* **1997**, *101* (24), 4798.
(14) Mellot, C.; Espinat, D. *Bull. Soc. Chim. Fr.* **1994**, *131* (7), 742–747.
(15) Mellot, C.; Espinat, D.; Rebours, B.; Baerlocher, C.; Fisher, P. *Catal. Lett.* **1994**, *27* (1−2), 159–169.
(16) Fajula, F.; Galarneau, A.; Di Renzo, F. *Microporous Mesoporous Mater.* **2005**, *82* (3), 227–239.
(17) Rowsell, J. L. C.; Yaghi, O. M. *Angew. Chem., Int. Ed.* **2005**, *44* (30), 4670–4679.
(18) Eddaoudi, M.; Li, H.; Yaghi, O. M. *J. Am. Chem. Soc.* **2000**, *122* (7), 1391–1397.
(19) Eddaoudi, M.; Moler, D. B.; Li, H.; Chen, B.; Reineke, T. M.; O'Keeffe, M.; Yaghi, O. M. *Acc. Chem. Res.* **2001**, *34* (4), 319–330.
(20) Fletcher, A. J.; Cussen, E. J.; Prior, T. J.; Rosseinsky, M. J.; Kepert, C. J.; Thomas, K. M. *J. Am. Chem. Soc.* **2001**, *123* (41), 10001–10011.
(21) Matsuda, R.; Kitaura, R.; Kitagawa, S.; Kubota, Y.; Belosludov, R. V.; Kobayashi, T. C.; Sakamoto, H.; Chiba, T.; Takata, M.; Kawazoe, Y.; Mita, Y. *Nature* **2005**, *436* (7048), 238–241.
(22) Barcia, P. S.; Zapata, F.; Silva, J. A. C.; Rodrigues, A. E.; Chen, B. L. *J. Phys. Chem. B* **2007**, *111* (22), 6101–6103.
(23) Chen, B.; Liang, C.; Yang, J.; Contreras, D. S.; Clancy, Y. L.; Lobkovsky, E. B.; Yaghi, O. M.; Dai, S. *Angew. Chem. Int. Ed.* **2006**, *45* (9), 1390–1393.
(24) Duren, T.; Snurr, R. Q. *J. Phys. Chem. B* **2004**, *108* (40), 15703–15708.
(25) Jiang, J.; Sandler, S. I. *Langmuir* **2006**, *22* (13), 5702–5707.
(26) Pan, L.; Olson, D. H.; Ciemnolonski, L. R.; Heddy, R.; Li, J. *Angew. Chem., Int. Ed.* **2006**, *45* (4), 616–619.
(27) Finsy, V.; De Bruyne, S.; Alaerts, L.; De Vos, D.; Jacobs, P. A.; Baron, G. V.; Denayer, J. F. M. *Stud. Surf. Sci. Catal.* **2007**, 2048–2053.
(28) Wang, Q. M.; Shen, D.; bülow, M.; Lau, M. L.; Deng, S.; Fitch, F. R.; Lemcoff, N. O.; Semanscin, J. *Microporous Mesoporous Mater.* **2002**, *55* (2), 217–230.
(29) Llewellyn, P. L.; Bourrelly, S.; Serre, C.; Filinchuk, Y.; Férey, G. *Angew. Chem., Int. Ed.* **2006**, *45* (46), 7751–7754.
(30) Dybtsev, D. N.; Chun, H.; Yoon, S. H.; Kim, D.; Kim, K. *J. Am. Chem. Soc.* **2004**, *126* (1), 32–33.
(31) Bastin, L.; Barcia, P. S.; Hurtado, E. J.; Silva, J. A. C.; Rodrigues, A. E.; Chen, B., A. *J. Phys. Chem. C* **2008**, *112* (5), 1575–1581.
(32) Bradshaw, D.; Prior, T. J.; Cussen, E. J.; Claridge, J. B.; Rosseinsky, M. J. *J. Am. Chem. Soc.* **2004**, *126* (19), 6106–6114.
(33) Wang, X.; Liu, L.; Jacobson, A. J. *Angew. Chem., Int. Ed.* **2006**, *45* (39), 6499–6503.
(34) Horcajada, P.; Serre, C.; Vallet-Reggi, M.; Sebban, M.; Taulelle, F.; Férey, G. *Angew. Chem., Int. Ed.* **2006**, *45* (36), 5974–5978.
(35) Alaerts, L.; Kirschhock, C. E. A.; Maes, M.; van der Veen, M. A.; Finsy, V.; Depla, A.; Martens, J. A.; Baron, G. V.; Jacobs, P. A.; Denayer, J. F. M.; De Vos, D. E. *Angew. Chem., Int. Ed.* **2007**, *46* (23), 4293–4297.
(36) Barthelet, K.; Marrot, J.; Riou, D.; Férey, G. *Angew. Chem., Int. Ed.* **2002**, *41* (2), 281–284.
(37) Schenk, M.; Calero, S.; Maesen, T. L. M.; van Benthem, L. L.; Verbeek, M. G.; Smit, B. *Angew. Chem., Int. Ed.* **2002**, *41* (14), 2499–2502.
(38) van Baten, J. M.; Krishna, R. *Microporous Mesoporous Mater.* **2005**, *84* (1−3), 179–191.
(39) Daems, I.; Leflaive, P.; Méthivier, A.; Baron, G. V.; Denayer, J. F. M. *Microporous Mesoporous Mater.* **2006**, *96* (1−3), 149–156.
(40) Daems, I.; Méthivier, A.; Leflaive, P.; Fuchs, A. H.; Baron, G. V.; Denayer, J. F. M. *J. Am. Chem. Soc.* **2005**, *127* (33), 11600–11601.
(41) Denayer, J. F. M.; Daems, I.; Baron, G. V. *Oil Gas Sci. Technol.* **2006**, *61* (4), 561–569.
(42) Denayer, J. F. M.; De Meyer, K.; Martens, J. A.; Baron, G. V. *Angew. Chem., Int. Ed.* **2003**, *42* (24), 2774–2777.

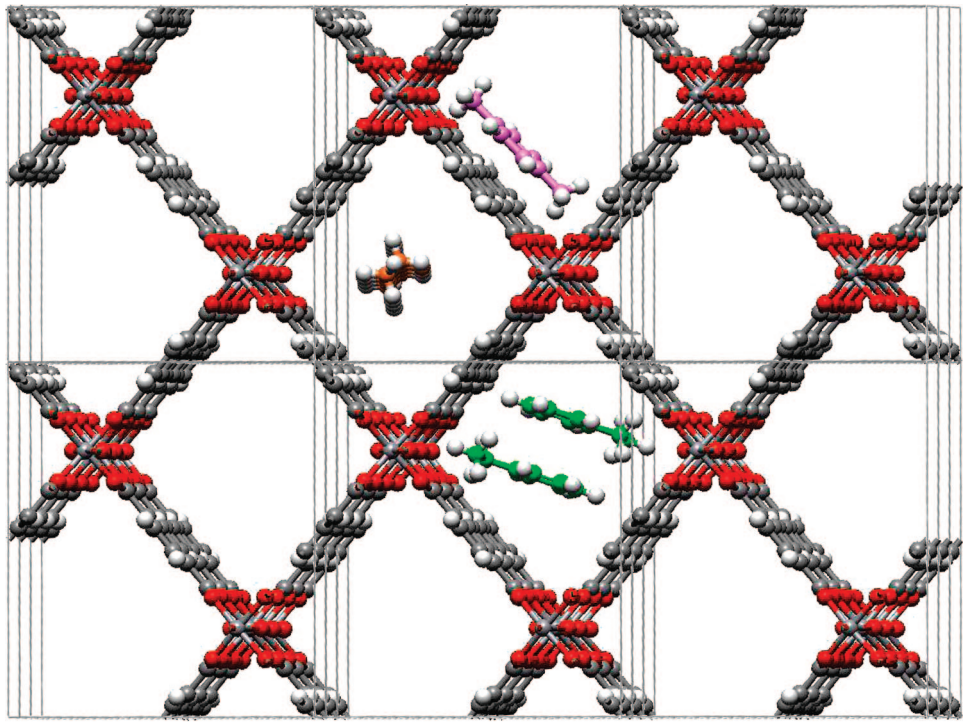

Figure 1. The MIL-47 framework with octane (orange), *p*-xylene (purple), and ethylbenzene adsorbed inside its unidimensional pores (grey lines indicate the borders of a unit cell).

Pulse Gas Chromatography. Zero coverage adsorption properties were determined using the pulse gas chromatographic method. Experiments were performed with *n*-pentane, *n*-hexane, *n*-heptane, *n*-octane, benzene, toluene, ethylbenzene, and *o*-, *m*-, and *p*-xylene. Stainless steel columns of 30 cm with internal diameters of 0.2159 cm were packed with binderless pellets of 500 to 630 μm. Prior to the measurements, the MIL-47 material was activated by heating to 300 °C at a heating rate of 1 °C/min in helium flow and keeping this final temperature over 10 h. Liquid pulses of 0.02 μL of the investigated components were injected in an inert carrier gas, He, flowing through a chromatographic column filled with MIL-47 pellets. At the column outlet, the response curve was measured with a thermal conductivity detector. Chromatograms were measured from 230 to 290 °C. Absence of diffusion limitations was verified by changing the carrier gas flow rate. Injections of different hydrocarbon volumes demonstrated that the experiments were performed in the linear part (Henry region) of the adsorption isotherm. Henry adsorption constants were calculated using the methods of moments.[43] Adsorption enthalpies were calculated from the temperature dependence of the Henry adsorption constants using the van't Hoff equation.

According to a localized adsorption model, the relationship between Henry adsorption constant K', adsorption enthalpy ΔH_0^{θ}, and adsorption entropy $\Delta S^{\theta}_{0,\mathrm{local}}$ takes the following form:[44,45]

$$K' = K_0' e^{-\Delta H_0/\mathrm{RT}} \tag{1}$$

with:

$$K_0' = \exp\left[\frac{\Delta S^{\Theta}_{0,\mathrm{local}}}{R} + \ln\left(\frac{n_\mathrm{T}}{2p^{\Theta}}\right)\right] \tag{2}$$

The subscript 0 refers to the zero coverage limit, p^{θ} refers to the standard state of the gas phase (1 atm), and n_T equals the number of adsorption sites. Thus, a plot of the preexponential factor of the van't Hoff equation $-\ln K_0'$ versus $-\Delta H_0$ reveals the relationship between adsorption entropy and adsorption enthalpy, or in other words the freedom lost for a given energetic interaction inside the pore system.

Breakthrough Experiments. Breakthrough experiments were performed using several chromatographic columns packed with MIL-47 pellets and with lengths of 15 or 30 cm and an internal diameter of 0.2159 or 0.4218 cm. A continuous total flow of 23 to 28 N mL/min. consisting of vaporized C8 alkylaromatic components in helium was generated by flowing He through metal reservoirs containing the liquid components. In order to control the vapor pressure, these reservoirs were conditioned in thermostatic baths. To obtain very low vapor pressures, the alkylaromatic−He stream could be diluted with He before entering the column. Doing so, total alkylaromatic partial pressures between 0.0004 and 0.05 bar were obtained at the column inlet. The gas stream at the outlet of the column was analyzed *online* with a gas chromatograph (GC) equipped with an automatic gas injection valve. A Stabilwax (crossbond Carbowax-PEG) column (Restek) with a length of 15 m, internal diameter of 250 μm and film thickness of 0.5 μm was used for the separation of the xylene mixture. Depending on the vapor pressure and the composition of the mixture, the concentration of the xylene isomers in the effluent could be measured every 1−2 min. Breakthrough experiments were performed at temperatures from 70 to 150 °C and at xylene partial pressures from 0.0002 to 0.02 bar.

The hydrocarbon partial pressure p_i is calculated with the Wagner equation:[46]

$$\ln\left(\frac{p_\mathrm{i}}{P_\mathrm{c}}\right) = (1-x)^{-1}[(\mathrm{VPA})x + (\mathrm{VPB})x^{1.5} + (\mathrm{VPC})x^3 + (\mathrm{VPD})x^6] \tag{3}$$

with:

$$x = 1 - \frac{T}{T_\mathrm{c}} \tag{4}$$

(43) Hufton, J. R.; Danner, R. P. *AIChE J.* **1993**, *39* (6), 954–961.
(44) Katsanos, N. A.; Kapolos, J.; Gavril, D.; Bakaoukas, N.; Loukopoulos, V.; Koliadima, A.; Karaiskakis, G. *J. Chromatogr. A* **2006**, *1127* (1−2), 221–227.
(45) Ocakoglu, R. A.; Denayer, J. F. M.; Marin, G. B.; Martens, J. A.; Baron, G. V. *J. Phys. Chem. B* **2003**, *107* (1), 398–406.

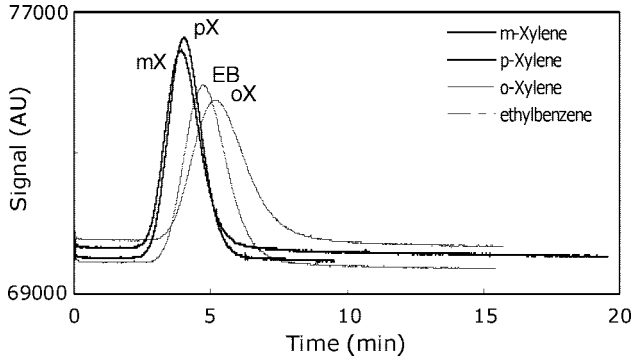

Figure 2. Chromatograms of C_8 alkylaromatic components on MIL-47 at 270 °C.

P_c refers to the critical pressure in bar, T and T_c the temperature and the critical temperature, respectively, in Kelvin, VPA, VPB, VPC, and VPD constants, all tabulated in reference.[46]

The adsorbed amounts q_i are calculated by integrating the experimental breakthrough curves. Since in the breakthrough experiment, the partial pressure of the adsorbing components varies during the experiment as a result of the ongoing adsorption process, only an apparent or average separation factor can be obtained. An average separation factor α, for a binary mixture of components i and j, is defined as:

$$\alpha = \frac{\left(\frac{q_i}{p_i}\right)}{\left(\frac{q_j}{p_j}\right)} \quad (5)$$

Vapor-Phase Isotherms. Vapor-phase adsorption isotherms were measured with the gravimetric technique using dedicated equipment of the VTI Corporation (Hialeah, FL). A reservoir, filled with the liquid hydrocarbon, is held at constant temperature through Peltier elements. He bubbling through the container entrains the organic vapor. This He−organic vapor streams continuously flows over the MIL-47 sample positioned in a sample holder connected to the microbalance. Adsorption isotherms of all C8 alkylaromatic components were determined at 70, 110, and 150 °C by weighing the xylene uptake at different partial pressures after activation of the MIL-47 sample by heating to 200 °C at a heating rate of 1 °C/min. This final temperature was kept until equilibrium was reached, with a maximum duration of 120 min.

Results

Low Coverage Adsorption Properties. Chromatograms obtained after injection of the individual C8 alkylaromatic isomers on a MIL-47 column at 270 °C are presented in Figure 2. Only small differences were observed with retention times differing maximally 27%. m- and pX, which are retained equally, elute first, followed by EB. oX is retained the longest. This order of elution of the C8 alkylaromatic components on the MIL-47 column does not follow the order of boiling points (EB: 136 °C < pX: 138 °C < mX: 139 °C < oX: 144 °C) as would be the case on a typical aspecific analytical chromatographic column. These differences in boiling points are so small that highly specific analytical columns have to be used for the separation of xylene isomers. Commercially available columns for xylene separation have stationary phases containing bound polyethylene glycol $H(OCH_2CH_2)_nOH$ which interact very strongly with polar components. The backbone O is responsible for a strong dipole interaction with the xylene isomers. For example, with the analytical column used in this work (Stabilwax) the order of elution was EB < pX < mX < oX, which indeed corresponds to the order of boiling points. Apparently, a different adsorption mechanism prevails on the MIL-47 material.

(46) Poling, B. E.; Prausnitz, J. M.; O'Connel, J. P. *The Properties of Gases and Liquids*, 5th ed.; McGraw-Hill Book Company: New York, 2000.

Table 1. Henry Constants (at 270°C) and Adsorption Enthalpy of All C_8 Alkylaromatic Components and *n*-Octane[a]

	T_{boil} (°C)	K'_{270} (mol/kg/Pa)	$-\Delta H_0$ (kJ/mol)
ethylbenzene	136	2.5×10^{-4}	59.7 ± 0.5
o-xylene	144	2.9×10^{-4}	59.6 ± 0.7
m-xylene	139	2.1×10^{-4}	59.7 ± 0.7
p-xylene	138	2.2×10^{-4}	61.2 ± 0.4
n-octane	126	2.2×10^{-4}	65.7 ± 0.6
o-xylene USY[b]		6.0×10^{-5}	65.3 ± 3.1
n-octane USY[b]		2.5×10^{-5}	56.5 ± 0.5

[a] Data for *n*-octane and *o*-xylene on USY zeolite (Si/Al 30) are added as reference. [b] From: Ph.D. dissertation Joeri Denayer, Vrije Universiteit Brussel, Belgium, Sept 1998, pp. 79.

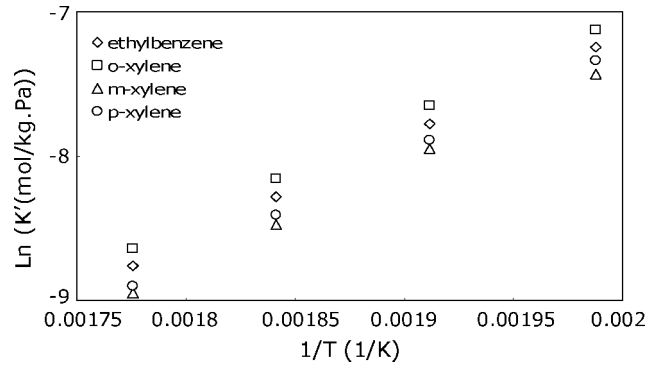

Figure 3. van't Hoff plot of ethylbenzene (◇), *o*-xylene (□), *m*-xylene (Δ), and *p*-xylene (○) on MIL-47.

Henry constants calculated from the experimental chromatograms of the C8 alkylaromatic isomers are reported in Table 1, together with the boiling points. For comparison, the Henry constant of *n*-octane on MIL-47 and oX and *n*-octane on a USY faujasite zeolite are added. In absolute terms, MIL-47 has Henry constants which are one to two orders larger in comparison to the USY zeolite and the mesoporous MCM-48. Henry constants of the C8 alkylaromatic isomers are comparable to the one of *n*-octane on MIL-47 whereas on USY, the Henry constant of oX is about 2.5 times larger than that of *n*-octane.

The temperature dependence of the Henry constants follows the van't Hoff equation as depicted in Figure 3. Zero coverage adsorption enthalpies calculated from the slope of the van't Hoff plots are tabulated in Table 1. oX, mX, pX, and EB interact with about the same strength with the MIL-47 framework. Remarkably, the adsorption enthalpy of the C8 aromatic components (about 60 kJ/mol) is significantly lower than that of *n*-octane (65.7 kJ/mol). Again, this is in clear contrast to what is commonly observed, i.e. a stronger interaction of the aromatic component compared to the saturated alkane (see Table 1 for USY). Whereas the adsorption enthalpy of *n*-octane is larger on MIL-47 compared to USY, the aromatic components have lower adsorption enthalpies on the former material. It thus appears that the π-clouds of the aromatics are not dominating the interaction with the MIL-47 framework. Rietveld refinement of MIL-47 samples fully loaded with o-, m-, and pX showed that these molecules adsorb with their aromatic ring not fully parallel to the aromatic ring of the terephthalate linkers in the

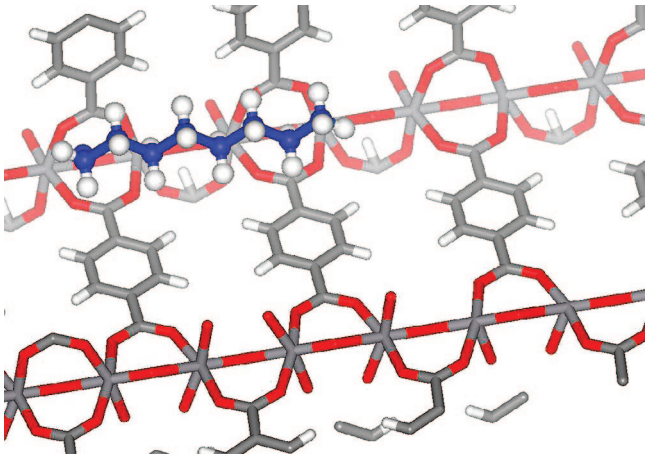

Figure 4. Schematic representation of a *n*-octane molecule in a MIL-47 pore. The hydrogen atoms (white) of *n*-octane are in close contact with the oxygen atoms (red) of the MIL-47 framework.

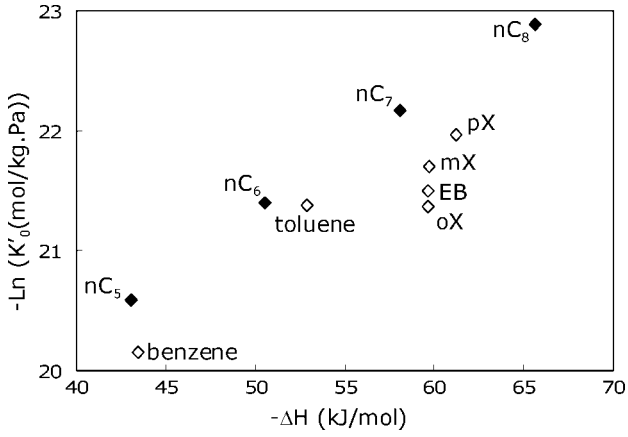

Figure 5. Compensation chart for linear alkanes (closed symbols) and aromatic components (open symbols) on MIL-47.

MIL-47 framework but in a rather skewed configuration as depicted in Figure 1.[35] Because of steric constraints, EB does not align at all with the phenyl rings of the terephthalate units at a high degree of pore filling but adopts a configuration in which there is a close interaction between the CH_3 group of EB and the terephthalate ligands. These observations suggest that interaction between the alkylaromatic hydrogen atoms and terephthalate oxygen framework atoms play an important role. Therefore, it is not unreasonable to suggest that the eight additional hydrogen atoms of *n*-octane compared to the C8 alkylaromatics lead to a stronger interaction. The linear octane molecule with its cylindrical shape can align itself with the longest axis of the pore channel, as shown in Figures 1 and 4. In this configuration, many of its hydrogen atoms are in close contact with the oxygen atoms of the framework, leading to a strong interaction, as visualized in Figure 4.

As expected, $-\ln K_0'$ varies in a linear way with $-\Delta H_0$ for linear alkanes (see Figure 5)[41,47] the longer the chain, the stronger the interaction between the molecule and the surface atoms in the MIL-47 pores, and in turn, the larger the loss of freedom. For USY, it has been observed that alkanes and aromatic components show the same relationship between adsorption enthalpy and entropy[48] (see Supporting Information).

For MIL-47, all points for the aromatic components fall below the line obtained for the *n*-alkanes. Considering eqs 1 and 2, this can be the result of a higher number of adsorption sites or a lower loss of entropy for the aromatics or even a combination of both. Concerning the contribution of entropy, it can be stated that both aromatics and linear alkanes only retain one degree of translational freedom, corresponding to a movement along the longitudonal axis of the one-dimensional pore. With respect to rotation, it is not easy to differentiate between alkanes and alkylaromatics. It could be speculated that for *n*-octane, only the rotation along the longest axis of the alkane chain is not sterically hindered and allows close contact between the alkane hydrogen atoms and the oxygen atoms of the framework. For the aromatics, more degrees of rotational freedom could be retained, but an independent study would be needed to verify this hypothesis. Regarding the number of adsorption sites, it is observed that the adsorption capacity of *n*-octane is only half of that of the alkylaromatics (vide infra). Whereas two alkylaromatics can be adsorbed in the radial direction of the pore, only one octane molecule is adsorbed in the same space.

Thus, it is concluded that in spite of a lower adsorption enthalpy, the C8 alkylaromatics have Henry adsorption constants similar to that of *n*-octane because they have a higher number of adsorption sites and possibly loose less freedom during adsorption in the pores of MIL-47.

Adsorption Isotherms. Adsorption isotherms of the C8 alkylaromatics and *n*-octane at 70 °C, 110 °C, and 150 °C are shown in Figure 6. Large adsorption capacities, up to almost 40 wt% at 70 °C were measured, corresponding to a pore filling degree of 3.4 molecules per unit cell or 1.7 molecules per channel segment (see Figure 1). At the same temperature, all isomers show a very steep isotherm. The largest adsorption capacity is measured for pX, in order followed by oX, mX, and EB. pX reaches its plateau at a partial pressure of 0.005 bar, but for the other isomers the amount adsorbed keeps on increasing over the whole experimental pressure range. It therefore cannot be ruled out that all C8 alkylaromatics reach the same adsorption capacity at sufficiently high pressures.

The observed tendencies can be related to the modes of packing of the C8 alkylaromatic molecules in the MIL-47 pore system as elucidated in earlier work by Rietveld refinement of the X-ray powder diffraction patterns of MIL-47 samples saturated with each of the isomers at room temperature and in the liquid phase.[35] It was found that all isomers adsorb in pairs along the length of the pores, with two pairs in every unit cell (Figure 1). This is in fair agreement with the maximal adsorption capacity of 3.4 molecules per unit cell as determined by gravimetry at 70 °C. The major difference between the molecular arrangements of the three xylene isomers is the relative alignment of the aromatic planes of the molecules within a pair. For pX, the aromatic rings of a pair are aligned in an almost perfect parallel configuration, with staggered methyl groups. For oX, the alignment of the aromatic rings is slightly less effective, explaining the lower steepness of the oX isotherm at 70 °C. With mX, steric interactions between molecules in neighboring unit cells cause a tilt and turn of the aromatic rings of the paired mX molecules in the same unit cell relatively to each other, preventing the paired mX molecules to align their aromatic rings in an optimal way. Thus both for mX and oX, a higher pressure is needed to achieve the same packing efficiency as compared to pX. Steric constraints in the pores caused by the ethyl group

(47) Ruthven, D. M.; Kaul, B. K. *Adsorption* **1998**, *4* (3−4), 269–273.

(48) Denayer, J. F. M.; Baron, G. V. *Adsorption* **2005**, *11*, 85–90.

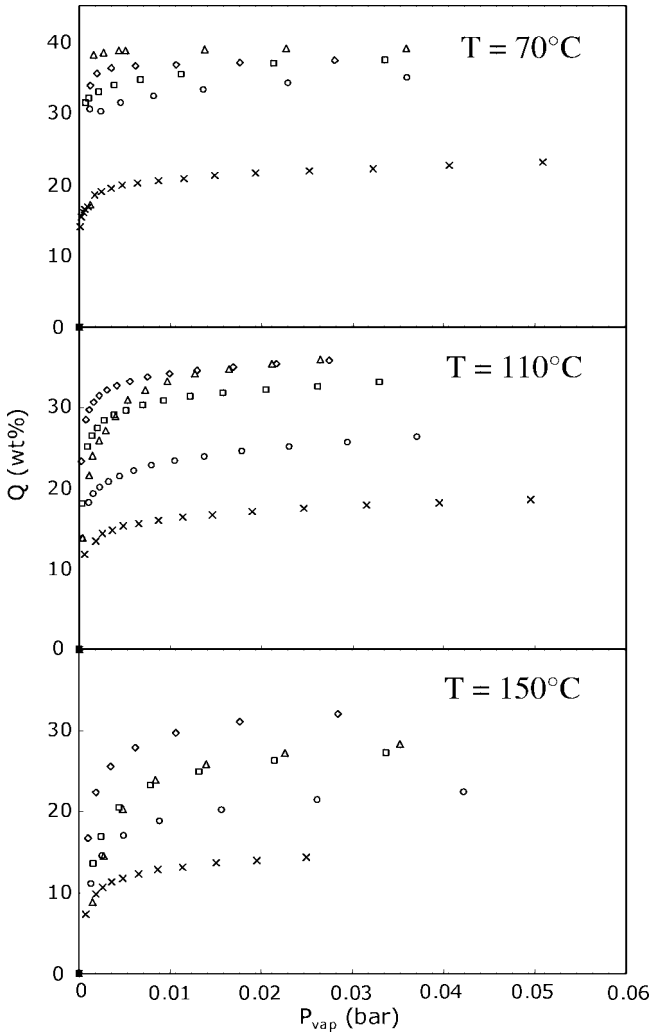

Figure 6. Adsorption isotherms for ethylbenzene (○), *p*-xylene (Δ), *o*-xylene (◇), *m*-xylene (□), and *n*-octane (x) measured at 70, 110, and 150 °C on MIL-47.

of EB prevents planar alignment of the aromatic rings, such that π-π interactions between EB molecules or EB molecules and the framework become insignificant. It was found that the methyl groups of EB are interacting with the terephthalate units, causing a distortion of the MIL-47 lattice. Both effects imply an energy cost which explains the significantly lower uptake of EB.

As expected, adsorption isotherms are less steep at 110 and 150 °C, but also the order of adsorption capacities and isotherm steepnesses is different from that at 70 °C. Both at 110 and 150 °C, oX has the steepest isotherm, whereas at 70 °C, *p*-xylene is adsorbed to the largest extent. At 110 °C, the pX isotherm is less steep than that of *m*-xylene at low pressures, but reaches a higher capacity at high pressure. At 150 °C, the *p*- and *m*-xylene isotherms almost coincide. The difference in amount adsorbed between the most strongly adsorbed isomer and the least strongly adsorbed isomer (ethyl benzene) grows larger with increasing temperature. For example at 150 °C, a capacity of 32 wt% or 2.8 molecules/unit cell is reached for oX, while EB reaches 22 wt% in the experimental pressure range, corresponding to only 1.9 molecules/unit cell. It should be noted that almost 3 EB molecules are adsorbed per unit cell at complete saturation at 70 °C. Possibly, a further increase in the amount adsorbed occurs at higher partial pressures.

It should thus be concluded that at higher temperatures (110 and 150 °C), the molecules pack in a subtly different way as compared to the conditions under which the Rietveld refinements were performed (room temperature). As a result of the higher thermal energy of the molecules, a dense and efficient packing becomes more difficult, leading to less steep isotherms and lower adsorption capacities.

Compared to the C8 alkylaromatic components, significantly smaller amounts of *n*-octane are adsorbed under all conditions, in spite of the higher adsorption enthalpy of this component (Table 1). *n*-Octane only reaches an adsorption capacity of 23 wt% or 1.9 molecules/unit cell at 70 °C (about 1 molecule per channel segment). This confirms the hypothesis that linear alkanes adsorb with their main carbon chain in the direction of the longest pore axis (see Figure 10). Because of steric constraints, only 1 alkane molecule fits in the cross section of the pore, limiting the adsorption capacity to 1 molecule per channel segment at maximum. The number of adsorption sites for the *n*-alkanes is only the half of that of the C8 alkylaromatics, readily explaining the lower preexponential factor of the former molecules (Figure 5).

Binary Breakthrough Experiments. Vapor-phase breakthrough experiments with a series of binary mixtures (mX/pX; EB/pX; oX/mX; oX/pX; oX/EB; mX/EB) were performed to determine the separation potential of MIL-47 in vapor-phase conditions. Breakthrough curves of the different equimolar mixtures at 70 °C and a total hydrocarbon pressure of 0.05 to 0.06 bar are shown in Figure 7.

All breakthrough profiles show an initial phase during which both components of the feed are fully adsorbed followed by a roll-up: the strongest adsorbed component displaces a part of the weaker adsorbed component, resulting in effluent concentrations temporarily higher than the feed concentration.

For the first mixture (pX/oX) almost no separation is observed, while the largest separation is obtained for the mX/pX mixture (third chart of Figure 7) under the present conditions. Thus with exception of the pX/oX mixture, a clear separation is achieved with the MIL-47 metal organic framework. For all mixtures containing EB, this component elutes first. Both mX and pX elute from the column before oX. For the mX/pX mixture, pX is the strongest adsorbed component. The following order of selectivities under mixture conditions can be derived from this set of experiments: oX $\sim$ pX > mX > EB, which is in fair agreement with the pure component isotherm observations.

Average separation factors calculated for these experiments are given in Table 2, together with ratios of Henry constants which are a measure for the separation at a very low degree of pore filling. In nearly all cases (except for the oX/mX and oX/pX mixtures), larger separation factors are obtained in the breakthrough experiments compared to the low coverage experiments. For two of the six mixtures (EB/pX and EB/mX) the selectivity is even reversed at high loading compared to zero loading. This shows that the separation of C8 alkylaromatics on MIL-47 is dependent on the degree of pore filling. Further experiments with mX/pX and EB/pX mixtures were performed to determine the effect of partial pressure or degree of pore filling and temperature on the separation behavior.

1. Effect of Temperature. Since the pure component isotherm experiments indicated a strong temperature effect, separation of binary mX/pX and EB/pX mixtures was studied at temperatures between 70 and 150 °C. Figure 8 depicts the relation between temperature and the average separation factor α for both mixtures. An optimum at about 110 °C is observed for

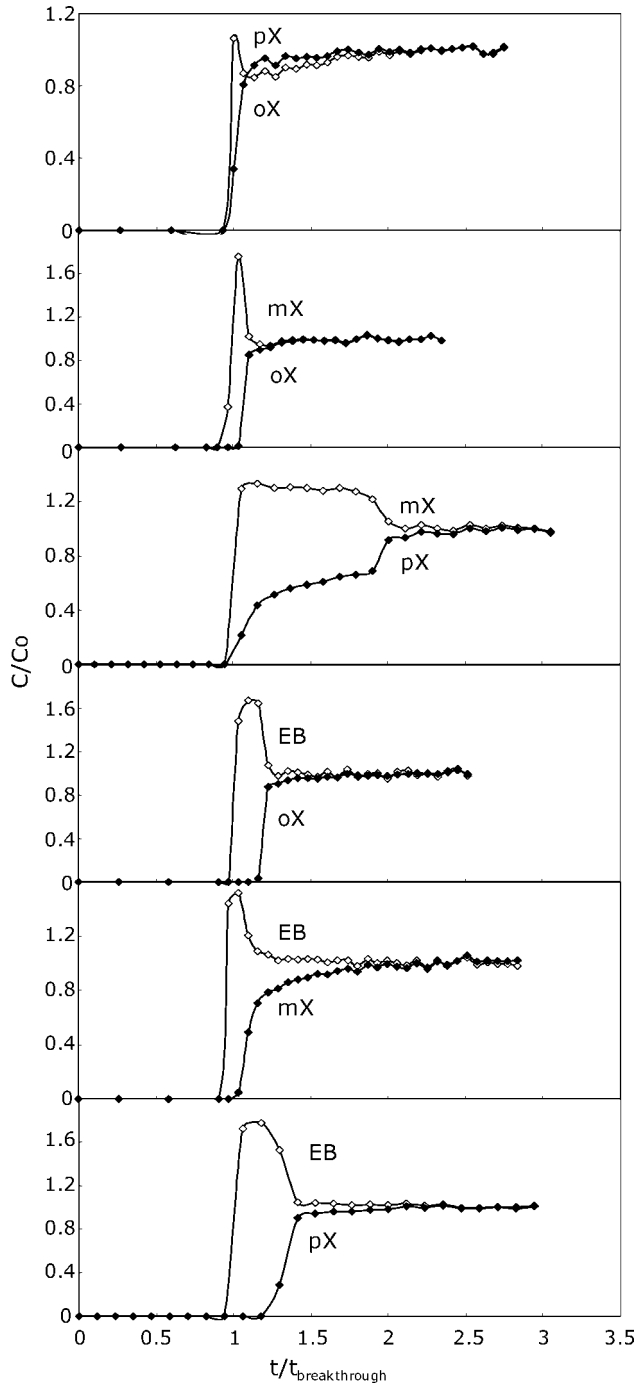

Figure 7. Breakthrough curves for the separation of equimolar binary C8 alkylaromatic mixtures at 70 °C and total hydrocarbon pressures of 0.05 to 0.06 bar. Experimental time was reduced by dividing by the time at which the least adsorbed component breaks through.

the separation of EB and pX, with average separation factors ranging from 1.6 to 3.4. For the separation of mX and pX, the selectivity decreases with temperature and reaches 1 at 150 °C, corresponding to nonselective adsorption. Interestingly, the pure component adsorption isotherms of m- and pX also coincide at 150 °C (see Figure 6).

2. Effect of Pore Occupancy. To obtain the largest possible separation, further experiments were carried out at 70 °C for the equimolar mX/pX mixture and at 110 °C for the equimolar EB/pX mixture. Figures 9 and 10 show the corresponding breakthrough curves at different pX pressures and constant temperature.

Table 2. Average Separation As Calculated from Binary Breakthrough Experiments at a Total Hydrocarbon Pressure of 0.05 to 0.06 Bar (α (breakthrough) and Zero Coverage Separation Factor Obtained by Dividing the Extrapolated Henry Constants (α (Henry Constant)) on MIL-47 at 70 °C

mixture	preferred component	α (breakthrough)	α (Henry Constant)
EB/pX	pX	1.83	0.97
EB/mX	mX	1.41	0.84
EB/oX	oX	1.39	1.13
mX/pX	pX	2.07	1.19
oX/mX	oX	1.17	1.35
oX/pX	−	1.01	1.11

For the mX/pX separation, elution of both components starts simultaneously at all partial pressures, pointing at a rather low selectivity. However, a clear evolution of the shape of the breakthrough curves with xylene partial pressure is appreciable. At very low partial pressure and thus low degree of pore filling, the pX and mX breakthrough curves are very steep and evolve rapidly to the feed concentration. From a pX partial pressure of 0.0065 bar, the shape of the pX and mX breakthrough profiles adopt an unusual shape. Three different phases can be observed after the initial phase in which both components are fully adsorbed. In phase I, a simultaneous and steep breakthrough of both components occurs. In phase II, the breakthrough profiles almost become flat. In phase III, finally the breakthrough profiles become steep again and evolve rapidly to the feed concentration level.

Figure 11 shows the average separation factors as a function of the degree of pore filling for these experiments. In the Henry region, at negligible pore occupancy, the separation factor is close to 1. The average selectivity increases with increasing degree of pore filling in favor of pX. The occurrence of the three stages in the breakthrough profiles can therefore be rationalized as follows. In the initial stage, when the "empty" MIL-47 material in the adsorption column is contacted with the pX/mX mixture, both components are adsorbed equally, as their Henry adsorption constants are comparable. Under these conditions, the aromatic molecules have enough free space in the empty pores to adopt their ideal configuration and optimize host−guest interactions, not hindered by the presence of nearby molecules. Thus in this stage, pX and mX travel at comparable velocity through the column and reach the column outlet simultaneously. As adsorption in the column continues, the pores of the material gradually become filled with C8 alkylaromatic molecules. From a certain point on, available free space in the

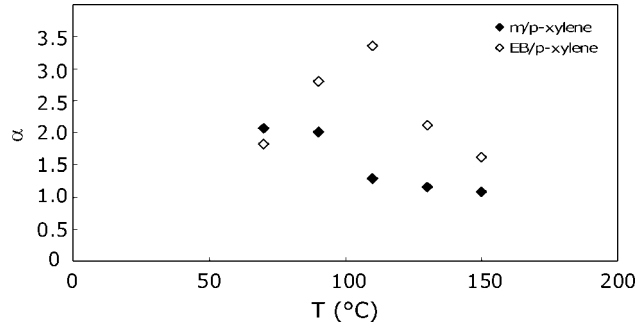

Figure 8. Temperature dependence of the average separation factor (α) for the separation of *m*-xylene/*p*-xylene (closed symbols) and ethylbenzene/*p*-xylene (open symbols) mixtures with MIL-47 at full loading.

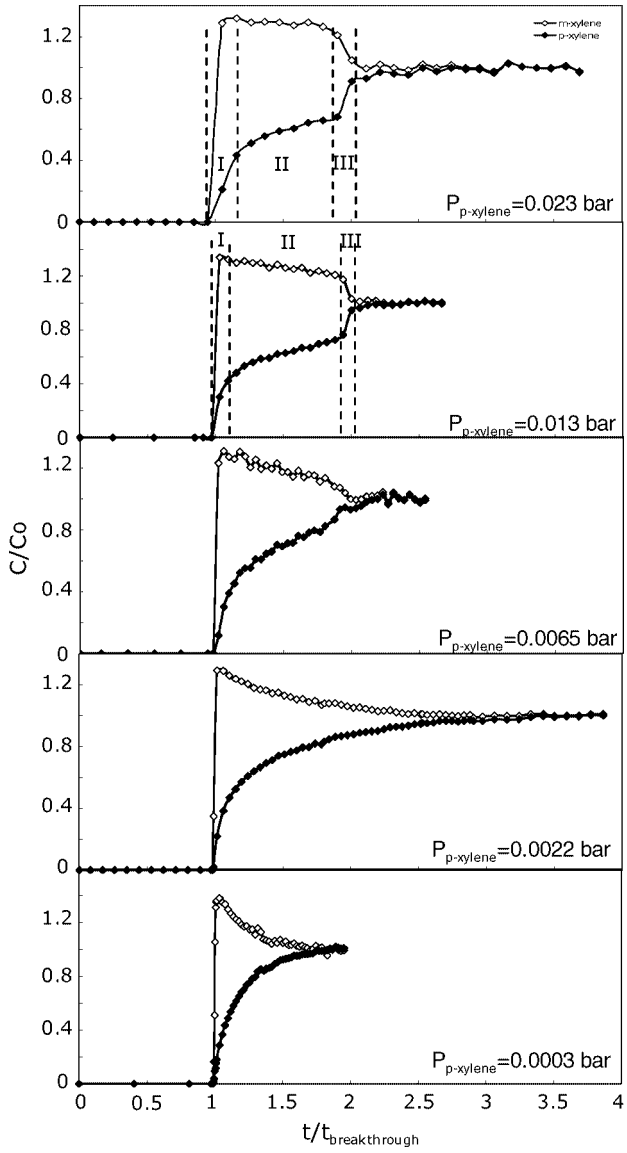

Figure 9. Breakthrough curves for the separation of *m*-xylene (open symbols)/*p*-xylene (closed symbols) mixtures at different vapor pressures and a temperature of 70 °C.

pores becomes critical. Efficient stacking of the molecules is required to fully occupy the available pore volume. As evidenced by Rietveld refinement of MIL-47 samples loaded with xylene isomers and the isotherm experiments, pX is stacked more efficiently and is capable of filling the pores at a lower energy cost as compared to mX. pX will be adsorbed selectively at the expense of mX when the degree of pore filling increases. This explains the change in shape of the breakthrough curves, where elution of pX is slowed down (phase II in Figure 9). This process continues until the pores are completely filled. At this point, no additional molecules from the feed are adsorbed and outlet concentrations evolve rapidly to the inlet concentrations (phase III).

For the EB/pX separation, also an initial simultaneous breakthrough of both components is observed at the lowest partial pressure. The EB concentration rises rapidly and exceeds the feed concentration whereas the pX concentration stays below its feed concentration. This corresponds to a preferential adsorption of pX, which is in disagreement with the order of Henry constants measured at infinite dilution, where EB is

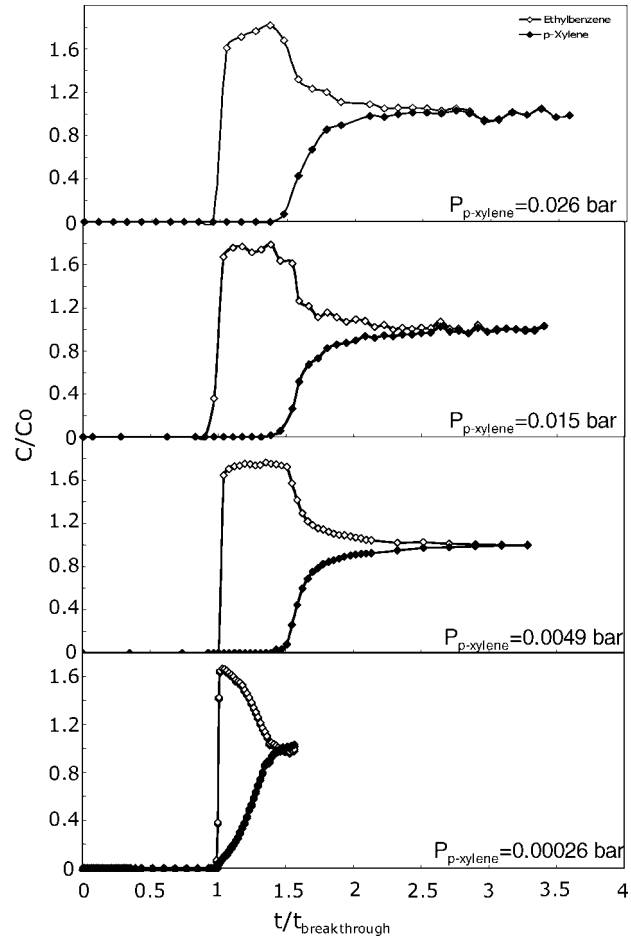

Figure 10. Breakthrough curves for the separation of ethylbenzene (open symbols)/*p*-xylene (closed symbols) mixtures at different vapor pressures and a temperature of 110 °C.

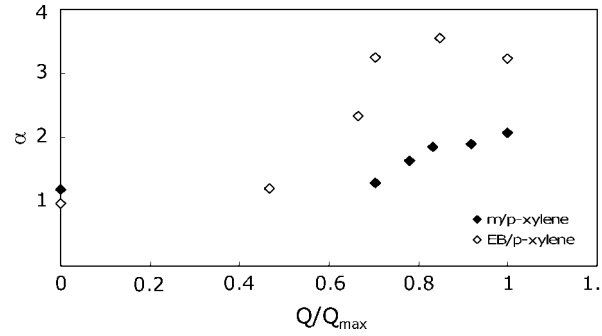

Figure 11. Effect of loading on the average separation factor (α) for the separation of equimolar *m*-xylene/*p*-xylene (closed symbols) and ethylbenzene/*p*-xylene (open symbols) mixtures at 70 and 110 °C respectively using MIL-47.

adsorbed more selectively compared to pX (Table 1). With increasing partial pressure, the differences in adsorption between pX and EB become more apparent; whereas no pure EB could be obtained at the lowest pressure, a significant difference in breakthrough time between EB and pX is observed at higher pressure. Figure 11 shows a sharp increase in overall performance of the MIL-47 MOF for the EB/pX separation at pore fillings larger than 40%, with average separation factors reaching about 3.4 at 75% pore filling and higher. The larger separation factors for the EB/pX mixture as compared to the mX/pX mixture are explained by the significantly less efficient packing

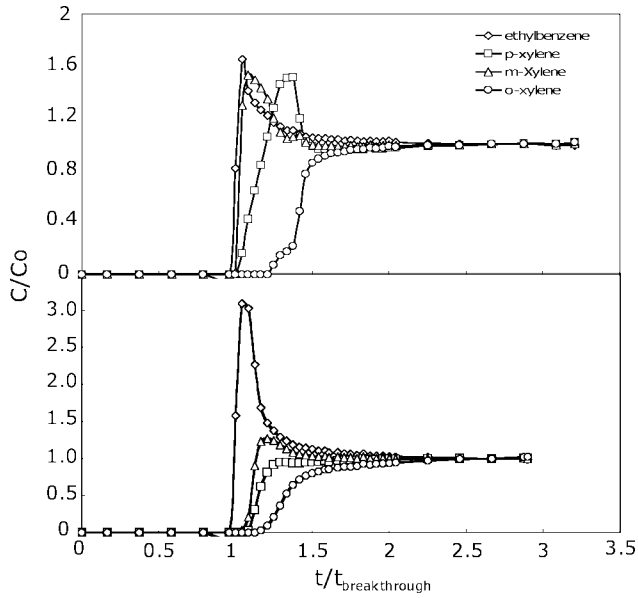

Figure 12. Separation of equimolar 4-component [ethylbenzene (◇), *o*-xylene (○), *m*-xylene (Δ), and *p*-xylene (□)] mixture with MIL-47 at 70 °C (top) and 110 °C (bottom) at a total hydrocarbon pressure of 0.05 bar.

of EB compared to the other C8 alkylaromatics (*vide supra*). Whereas for the EB/pX separation, the average separation factor reaches a maximum, the average selectivity keeps increasing with loading for the mX/pX separation.

Quaternary Breakthrough. Figure 12 shows the separation of an equimolar mixture of pX, mX, oX, and EB at 70 and 110 °C. Again a large effect of temperature on selectivity was observed. At 70 °C, mX and EB elute first and are not separated from each other in the present conditions. pX elutes as athird component and is clearly separated from oX, the most strongly adsorbed component. This order of elution corresponds to the order of selectivities as determined at 70 °C from the binary adsorption experiments. The breakthrough curve of oX shows a stepwise profile, similar to the stepwise shape of the binary breakthrough experiments, pointing at a variation of adsorption selectivity with degree of pore filling. At 110 °C, the 4 C8 alkylaromatics are separated from each other. EB elutes first followed by mX, pX, and oX. The better separation of EB and mX at 110 °C is in accordance to the larger differences in their pure component isotherms at 110 °C as compared to 70 °C (see Fgure 6).

Conclusions

In this work, gas-phase adsorption of C8 alkylaromatics on the metal−organic framework MIL-47 is studied. In the Henry region, at very low partial pressure, *p*-xylene, *m*-xylene, *o*-xylene, and ethylbenzene have comparable Henry adsorption constants and adsorption enthalpies. The relatively low value of the adsorption enthalpy of aromatics on MIL-47 in comparison to zeolites points at a rather unspecific interaction and is beneficial with respect to the operation of adsorption processes in view of the ease of adsorbent regeneration at low energy cost. In spite of their comparable Henry constants and adsorption enthalpies, the individual C8 alkylaromatics have different adsorption capacities and isotherm shapes. This is a result of differences in ease with which the components can be packed in the sterically constrained environment of the MIL-47 pores. These differences in packing mode can be exploited to achieve molecular separation as was shown by performing breakthrough experiments with binary and quaternary mixtures. The adsorption selectivity increases with degree of pore filling, i.e. the more molecules are present in the pores the more the ordering of these molecules becomes important. As a result, adsorption selectivity is strongly dependent on pressure and temperature, which provides a powerful tool for the optimization of the adsorptive separation process.

Acknowledgment. Luc Alaerts and Joeri Denayer are grateful to F.W.O.-Vlaanderen (Research Foundation—Flanders) for positions as a research assistant and postdoctoral researcher, respectively. This work was performed in the frame of the IAP Functional Supramolecular Systems of the Belgian Federal Government. Joeri Denayer is grateful to F.W.O.-Vlaanderen (Research Foundation—Flanders) for financial support for the gravimetric adsorption system used in this work.

Supporting Information Available: Figure S1 shows the compensation plot of *n*-alkanes and aromatics on NaY and NaUSY. This material is available free of charge via the Internet at http://pubs.acs.org.

JA800686C